ELSEVIER

Polymer 43 (2002) 2267–2277

polymer

www.elsevier.com/locate/polymer

Effects of phase separation on stress development in polymeric coatings

D.M. Vaessen, A.V. McCormick, L.F. Francis*

Department of Chemical Engineering and Materials Science, University of Minnesota-Twin Cities, Minneapolis, MN 55455-0132, USA

Received 19 October 2001; received in revised form 27 December 2001; accepted 31 December 2001

Abstract

A cantilever deflection technique was used to monitor stress in situ during drying of cellulose acetate coatings. Porosity was introduced in some coatings using dry-cast phase separation. Stress and weight loss profiles for dense coatings, a coating that contained small (~1 μm) pores, and a coating that contained small (~1 μm) pores and macrovoids (~200 μm) are compared. In-plane tensile stress after drying ranged from 30 MPa (dense coatings) to 5 MPa (macrovoid-containing coating). The stress profiles for dense coatings feature a period of rapidly and then slowly increasing stress due to constrained shrinkage. For a coating that formed small pores, drying and stress development are delayed, stress rises and then drops a small amount due to capillary pressure relief. The stress profiles for the small pore and macrovoid-containing coatings are similar, except for a stress plateau at early stages of drying, which may be caused by macrovoid growth. © 2002 Published by Elsevier Science Ltd.

Keywords: Dry-phase separation; Coating stress; Porosity

1. Introduction

Industrial coating formulations often contain mixtures of solvents in order to control drying rate, induce phase separation and porosity, lower cost, and alter surface tension [1–3]. For some coatings, the goal is to maintain the polymer solution coating as a single phase during the entire drying process until it gels or vitrifies into a dense structure [4]. On the other hand, for many asymmetric, porous polymeric membranes, the goal is to induce phase separation and subsequent porosity [5–7]. Phase separation can be induced in several ways: solvent evaporation (the 'dry-cast process'), immersion in a nonsolvent (the 'wet-cast process'), and thermal induced phase separation (TIPS). In this work, the dry-cast process is used to generate porosity in polymer coatings. During the dry-cast process, a three-component mixture consisting of a polymer, a volatile solvent, and a less volatile nonsolvent is coated onto a substrate and then dried. As evaporation of solvent takes place, the composition enters the two-phase region in the ternary phase diagram and phase separation occurs, producing a polymer-rich phase that forms the rigid membrane structure and a polymer-lean phase that eventually becomes the membrane pores [8,9]. This report explores the effects of phase separation from solvent evaporation on coating stress.

Asymmetric membranes are used in a variety of industrial applications including microfiltration, ultrafiltration, reverse osmosis, and gas separation [7–12]. These membranes usually consist of a very thin (0.1–1 μm) dense polymer layer (skin) on a highly porous 25–200 μm-thick sublayer. The microstructure (i.e. thickness of skin, pore size, and pore size gradients) of a membrane made by the dry-phase separation route is known to depend on the choice of polymer, the choice of solvent and nonsolvent, the composition of the polymer solution, the gelation and crystallization behavior of the polymer, the location of the liquid–liquid demixing gap, and the temperature of the polymer solution [7,8]. Unfortunately, the conditions chosen to produce a skin with desired properties for membrane operation sometimes lead to the formation of large macrovoids in the support. Macrovoids are comparatively large pores (10s or 100s of microns) that can extend through the thickness of the membrane. They have been observed in membranes prepared by both dry- and wet-phase separation [6–9, 11–18]. In general, macrovoids are not desired because they cause mechanical weaknesses in the sublayer and cause the membrane to tear during use [7,8]. One motivation for conducting the present study is to understand the possible role of coating stress on macrovoid formation; coating stress has already been found to lead to defects such as peeling, curling, cracking, crazing, rippling, and bending [19–22].

Stress develops in coatings prepared from liquid solutions

* Corresponding author. Tel.: +1-612-625-0559; fax: +1-612-626-7246.
E-mail address: lfrancis@tc.umn.edu (L.F. Francis).

0032-3861/02/$ - see front matter © 2002 Published by Elsevier Science Ltd.
PII: S0032-3861(02)00042-3

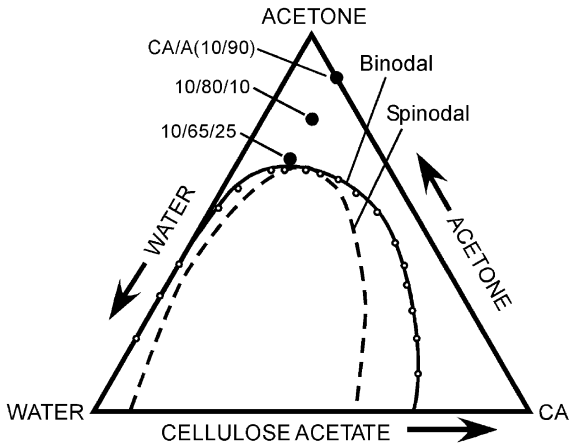

Fig. 1. Ternary phase diagram for cellulose acetate, acetone, and water showing initial polymer solution compositions used. Cloud point data (binodal) measured at 25 °C [10] and dashed line is a guess of the spinodal boundary.

as the liquid is transformed into an elastic or viscoelastic solid. For a drying coating, large volume changes (i.e. shrinkage) occur due to solvent evaporation. If the coating adheres to a rigid substrate, shrinkage (after solidification) can only occur in the thickness direction. Frustration of in-plane shrinkage leads to a tensile coating stress. However, at the same time that stress accumulates, it may be relaxed by processes such as molecular motion and flow. The measured stress at any time is the result of the competition between stress buildup from frustrated shrinkage and stress relief from relaxation.

A number of processing variables have already been shown to affect stress development during drying of binary (polymer/solvent) coatings that do not develop porosity: temperature, relative humidity, coating thickness, initial composition, and pigmentation [19–21,23–27]. However, the effect of adding a third component (a second solvent or a nonsolvent) on stress has received little attention, especially in coatings that develop porosity due to phase separation. The main focus of this paper is to measure the stress in coatings that develop porosity during drying. The effects of stress on macrovoid formation are also considered. For comparison, however, the coating stress evolution of a ternary system that does not phase separate nor develops porosity is described. Weight loss data, time points when optical changes occur, and final microstructure images accompany most stress results. The research here will allow for a better understanding of why stresses develop in porous coatings and how such stresses can be controlled.

2. Experimental

2.1. Materials and initial solution compositions

Cellulose acetate (CA) (CA-394-60S; Eastman Chemical Products, Inc., Kingsport, TN) was used as the polymer. Two different solvents were used: (1) reagent grade ACS/USP acetone 99.5 + % (Pharmco, Brookfield, CT) and (2) 1,4-dioxane 99 + % (Aldrich Chemical Co., Milwaukee, WI). For phase separating coatings, deionized water (MillQ-grade, 18 MΩ) was the nonsolvent.

In this paper, we first examine the stress and weight loss behavior for a coating prepared from a simple binary polymer solution consisting of 10 wt% cellulose acetate (CA) and 90 wt% acetone (A); this coating remains dense during drying. The effects of adding a second, less volatile, solvent, are then considered. Dioxane (D) was chosen as a second solvent for two reasons. First, cellulose acetate, acetone, and dioxane are miscible in all proportions such that a coating prepared from these three components remains dense during the entire drying process. Therefore, the stress and weight loss profiles for the ternary CA/A/D coating can readily be compared with those of the binary CA/A coating, without the added complexity of phase separation and porosity development occurring. Secondly, because dioxane has about the same volatility as water (W) ($P^{sat} = 35$ mm Hg for dioxane and $P^{sat} = 20$ mm Hg for water at 22 °C), the stress and weight loss profiles for the dense CA/A/D coating can effectively be compared to those for a CA/A/W coating, which phase separates and develops small pores during drying. The initial composition of the ternary solution that did not phase separate during drying was 10 wt% CA, 80 wt% A, and 10 wt% D, and the initial composition of the ternary solution that phase separated and developed small pores during drying was 10 wt% CA, 80 wt% A, and 10 wt% W. In Section 3.3, the stress and weight loss profiles of a coating initially containing 10 wt% CA, 65 wt% A, and 25 wt% W (10/65/25) are considered; both small and large pores formed during drying of this coating. Fig. 1 shows the initial solution compositions for the binary CA/A coating and the two phase-separating coatings on a ternary phase diagram. All initial solution compositions and notations are summarized in Table 1. The components were mixed and stirred overnight before preparing the coatings.

Table 1
Solution compositions (wt%s) used in preparing cellulose acetate (CA) coatings

	CA	Acetone	Water	Dioxane	Notation
Non-phase-separating	10	90	–	–	CA/A
	10	80	–	10	CA/A/D
Phase-separating	10	80	10	–	CA/A/W (Section 3.2) or 10/80/10 (Section 3.3)
	10	65	25	–	10/65/25

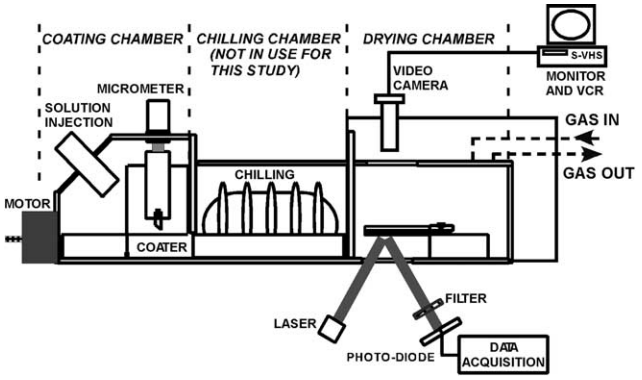

Fig. 2. Schematic of the stress apparatus, a controlled environment combination draw down coater, cantilever stress measurement system, and video camera.

2.2. Stress measurement

Stress development was monitored using a controlled environment stress measurement apparatus (Fig. 2) based on the cantilever deflection measurement principle [28]. An automated draw-down coater was used to meter coating thickness at a constant coating speed (0.50 cm/s). The blade gap was 300 μm for all coatings. Deflection was measured with an optical lever consisting of a small HeNe laser, a position sensitive photodiode (#DL-10; UDT Sensors, Inc., Hawthorne, CA), and various intermediary optics. The average in-plane stress in the coating is calculated from the cantilever beam bending equation:

$$\sigma = \frac{E_s t^3 d}{3cL^2(t+c)(1-\nu_s)} \quad (1)$$

where E_S and ν_S are the Young's modulus and Poisson's ratio of the substrate, respectively; t and L are the thickness and clamped length of the substrate, respectively; c is the coating thickness, and d is the end deflection of the cantilever. Although the coating thickness decreases during drying, it is not expected to change drastically after solidification when stress becomes measurable; therefore, the final coating thickness was used in the calculation of stress (c) and was measured with a micrometer (#543-253B, #7004; Mitutoyo Corp., Naucalpan, Estado de Mexico). For all experiments, the final coating thickness was less than 1/4 the substrate thickness, an assumption used in deriving Eq. (1). This derivation, along with assumptions and experimental constraints, is given elsewhere [27–32]. Note that only an average coating stress can be determined with this method; stress distributions throughout the coating thickness or in the plane of the substrate cannot be measured. For this reason, thinner coatings (compared to those produced in industrial membrane processes) were desired in this study to minimize the gradients in composition and stress through the thickness.

It is crucial to have good adhesion between the coating and substrate in order to measure coating stress via the cantilever deflection method. Various substrates and surface treatments were necessary to ensure adhesion throughout the entire drying process. The coatings prepared from CA/A and CA/A/D were applied onto 0.400 mm (±0.005 mm)-thick silicon substrates (Virginia Semiconductor, Fredericksburg, Virginia) that were sonicated in acetone for 15 min. All coatings prepared from the solution with composition 10 wt% CA/80 wt% A/10 wt% W were applied onto silicon substrates that were sonicated in acetone for 15 min, soaked in a 0.0001 M solution of benzyl methyl di-stearyl ammonium chloride in cyclohexane for 5 min, dried at room temperature for 1 h, and then dried in a 110 °C oven for 30 min. The coatings prepared from the solution with composition 10 wt% CA/65 wt% A/25 wt% W were applied onto 0.350 mm (±0.005 mm)-thick steel feeler gauge stock (L. S. Starrett Co., Athol, MA) which had been presoaked in isopropanol (>1 day) and dried in air for 30 min at room temperature. The clamped length of substrates in all cases was 45 mm (±0.5 mm), and the width was 6.5 mm (±0.5 mm).

For all experiments, drying took place at room temperature (21.5 ± 1.0 °C) under a 0% relative humidity nitrogen environment. The flow rate of nitrogen into the drying chamber was 1 LPM. The entire apparatus was purged ~30 min prior to coating application; therefore, both the coating and drying processes took place under a relative humidity-controlled environment.

2.3. Optical monitoring

Coatings that phase separated during drying change from transparent to translucent to opaque; for these coatings, video was recorded with a camera (#KP-D5O; Hitachi Ltd, Tokyo, Japan), monitor (#CT-S1390Y; Panasonic, Secaucus, NJ), and VCR (SVHS AG-1980; Panasonic, Secaucus, NJ) in order to correlate optical changes with changes in stress. These images were acquired at the same time stress measurement experiments were conducted.

2.4. Weight loss

Weight loss during drying was measured using an analytical balance (AG 245; Mettler Toledo Inc., Columbus, Ohio), fitted with a data transfer mechanism, in the configuration shown in Fig. 3. Substrates were coated in the lab using a draw down blade (~2 cm/s) and then quickly transferred (<10 s) to the weighing platform in the stress measurement chamber. Data was recorded automatically at defined intervals. Weight loss measurements were conducted inside the stress chamber to ensure the same experimental conditions; however, it was not possible to conduct stress experiments and weight loss experiments simultaneously. For this reason, the timescales for stress and weight loss do not match up exactly; the weight loss data lags (5–10 s) behind the stress data. This time lag is not significant on the time scale of these experiments, except at early times in the log scales of Figs. 8 and 11.

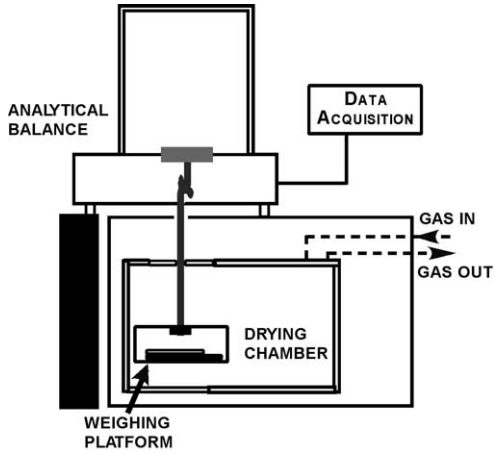

Fig. 3. Schematic of analytical balance, which was fitted to the stress apparatus drying chamber.

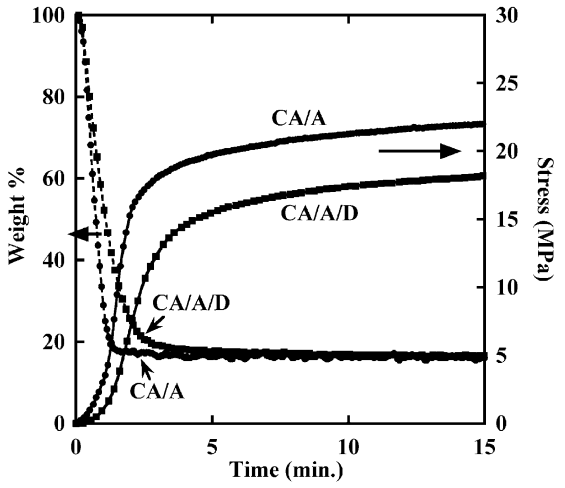

Fig. 5. Stress evolution (—) and weight loss (- - -) as a function of drying time for two non-phase-separating coatings of CA/A (10/90) (●) and CA/A/D (10/80/10) (■). Final thickness for both coatings was ~20 μm.

2.5. Microstructure

The microstructures of the dried coatings (after stress measurement experiments) were examined using scanning electron microscopy (SEM). Entire coatings were removed from substrates using a razor blade. They were then frozen in liquid nitrogen, where they became brittle enough to fracture into smaller pieces to expose cross-sections. The freeze-fractured samples were coated with a conductive 100 Å layer of platinum and then mounted on an SEM stub. A Hitachi S800 SEM with a field emission gun and a 5 kV voltage was used to acquire the final microstructure images.

3. Results and discussion

3.1. Addition of a second solvent

In this section, the evolution of coating stress and weight loss for the binary (CA/A) coating is compared with that of the ternary (CA/A/D) coating. Phase separation did not occur in either system; both coatings remained transparent throughout the entire drying process. This result is consistent with the results from the Flory–Huggins model using solubility parameters. Fig. 4 shows that final microstructure of the coating prepared from the CA/A/D solution is dense, except for a few scattered small voids (for comparison, Figs. 7A and 10D show the final microstructures of the porous coatings that phase separated during drying).

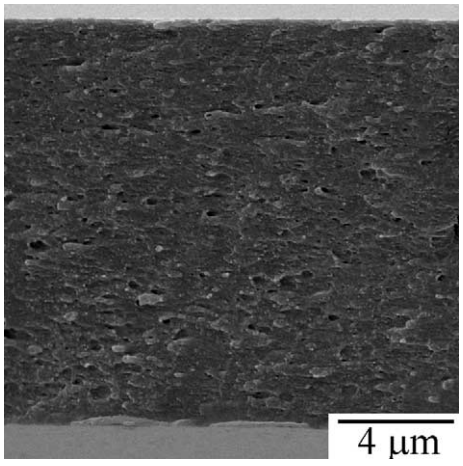

Fig. 4. SEM cross-section image showing final microstructure of the coating prepared from of CA/A/D (10/80/10).

Fig. 5 shows stress evolution curves and drying curves for cellulose acetate coatings prepared from binary and ternary solutions. For both coatings, an initial short period is observed during which no stress develops and weight loss is rapid. A tensile coating stress becomes apparent at around the 12 and 25 s time points for the binary and ternary systems, respectively. After this point, coatings continue to dry and stress increases first gradually and then more rapidly with time. Later, the rate of stress increase drops as drying slows considerably. At the end of the measurement (~16 h), the ternary CA/A/D coating has a tensile stress of ~23 MPa and the binary CA/A coating has a tensile stress of ~28 MPa. The final average coating thickness was ~20 μm for both coatings. Key differences between coatings are: (i) drying is more rapid and stress is apparent earlier in the coating prepared from the binary solution, and (ii) the final coating stress is higher in the coating prepared from the binary solution.

Stress development in drying polymer coatings results from constrained shrinkage. Assuming elastic behavior, coating stress (σ) can be related to post-solidification linear strain (ϵ) by

$$\sigma = \frac{E_c}{1 - \nu_c}\epsilon \tag{2}$$

where E_c and ν_c are the elastic modulus and Poisson's ratio of the coating, respectively [19,25]. The strain (ϵ) in a

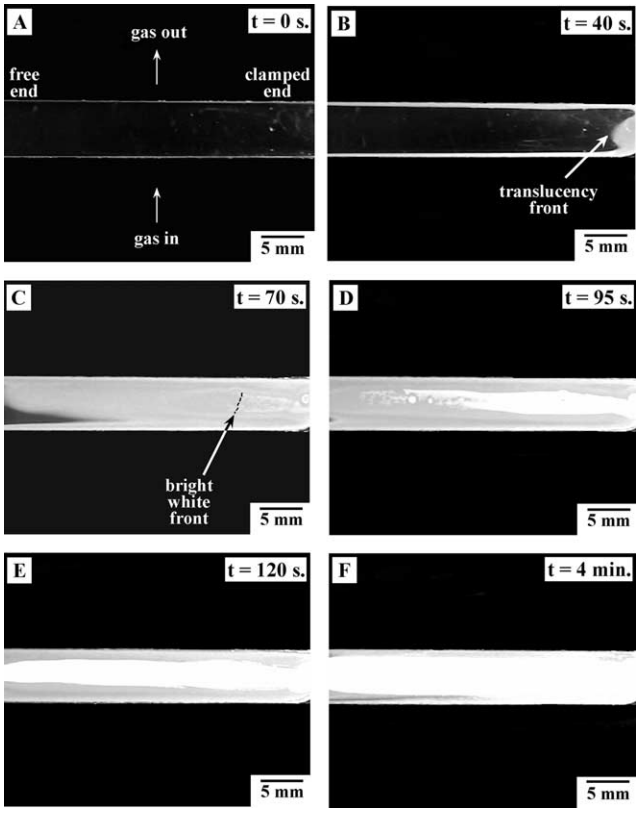

Fig. 6. Images of the surface of a coating prepared from CA/A/W (10/80/10), captured from a real time video. Time points indicated in the upper right of each image.

drying coating depends on the difference between the solvent content at the point of solidification and the solvent content at the end of drying. Solidification occurs roughly when the glass transition temperature of the coating is the same as the drying temperature. Inherent in this simple description is the fact that all solvent loss leads to shrinkage. The coating modulus in a drying coating is time-dependent and rises as drying proceeds. Therefore, the stress measured at any point during drying depends on accumulated effects of shrinkage from solvent loss and modulus rise up to that point.

From Fig. 5, solvent evaporation occurs rapidly at first and no coating stress is measured because the coating is still liquid. As drying proceeds, the elastic modulus (E_c) of the liquid coating grows until the coating becomes solid-like and is able to support stress. The CA/A coating supports a stress earlier than the CA/A/D coating because acetone, the only solvent, evaporates more quickly compared to the mixed solvent system. As drying proceeds further, even greater levels of stress per amount of shrinkage-induced strain are produced because evaporation also causes the coating modulus to rise. Toward the later stages of drying, stress continues to climb even though solvent evaporation is slow because the coating modulus is high.

Several factors may be responsible for the difference in the final stress of the two coatings. The ternary coating contains a less volatile solvent (dioxane) that is largely retained in the coating until the latter stages of drying. This second solvent may act as a plasticizer, keeping the coating modulus lower and hence stress lower as drying proceeds. In addition, the final removal of dioxane from the ternary coating may be less complete compared with the removal of acetone alone. To test this hypothesis, the following study was conducted: coatings prepared from the binary and ternary systems were dried ~15 min (the amount of time it took for the weight percents to appear equal in Fig. 5) while stress data was recorded. The coatings were then weighed, and further dried in an oven at 180 °C for ~2 h, and then reweighed. From this study, it was found that 10% and 16% of the coating weight at the 15 min time point was solvent in the binary and ternary coatings, respectively. Therefore, even though the weight percents plotted in Fig. 5 (which are based on the initial coating weight) appear almost the same during the latter stages of drying, there are differences in amount of solvent retained. Lastly, the specific volume of dioxane (0.886 cm^3/g) is less than that of acetone (1.27 cm^3/g); hence, the amount of shrinkage strain in the ternary system is smaller.

There are differences in final stress and the time to solidify in the dense CA/A and CA/A/D coatings; however, the stress profiles for these dense coatings are roughly the same. The stress profiles can be broken into three regimes: (1) at early stages of drying, stress is zero while weight loss is occurring very rapidly (coating is a liquid), (2) after 'solidification', stress increases rapidly, while weight loss is occurring less rapidly (than in regime (1)), and (3) at late stages of drying, stress increases slowly, while weight loss occurs slowly (vitrified coating).

3.2. Addition of a nonsolvent

In this section, the effects of phase separation and porosity are considered by comparing stress and weight loss for a CA/A/D coating with a CA/A/W coating, which phase separates. The initial polymer solution composition was 10 wt% CA, 80 wt% A, and 10 wt% dioxane (D) (or 10 wt% water (W)) and the coatings were dried under 0% RH.

Fig. 6 shows the images of the surface of the CA/A/W coating (obtained with a video camera) during drying. Initially, the coating is transparent because it is still a one-phase homogenous polymer solution; however, after 40 s of drying, 0.5 mm zones of translucency appear near the coating edges and translucency also starts to become visible near the clamped end of the substrate. A translucency front sweeps from the clamped end, which was coated first, to the free end such that the entire coating is translucent by the 100 s time point. The translucent appearance of the coating indicates that the composition at some depth in the coating has entered the two-phase region in the ternary phase diagram (i.e. phase separation has occurred); the two phases have different indices of refraction and visible light is scattered [33]. Translucency becomes apparent near the edges

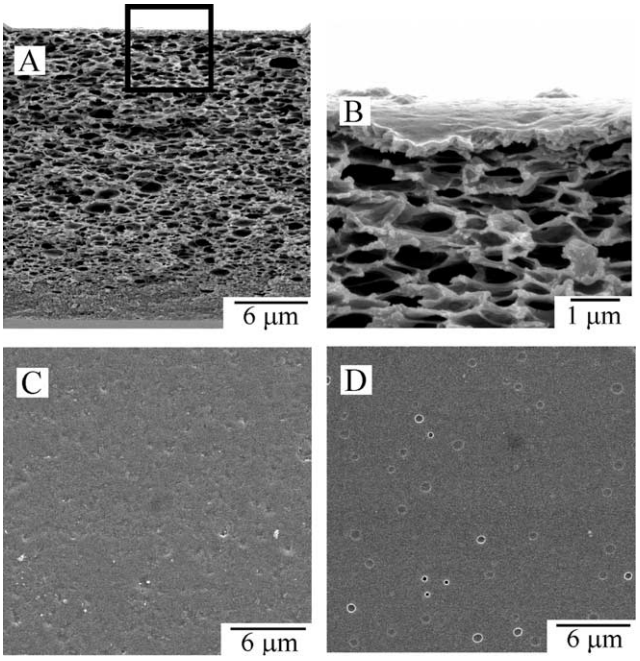

Fig. 7. SEM images showing the final microstructure of the coating prepared from CA/A/W (10/80/10): (A) cross-sectional image of entire coating; (B) cross-sectional image showing the skin (black box in 7(A)); (C) top coating surface; (D) bottom coating surface.

first because the coating is thinner there and dries faster, causing the composition to enter into the two-phase region earlier. The clamped end turned translucent before the free end because it was coated first and begins to dry first. At around the 70 s time point, the coating begins to change from translucent to bright white, again starting at the clamped end. A bright white front moves down the center portion of the coating, and then gradually moves outward toward the edges. The bright white appearance is likely due to the evaporation of the polymer-lean phase, leaving pores that contain air [33]. It is difficult to detect the exact time when the entire coating is bright white because the front moves more slowly as it reaches the edges of the coating; however, a good estimate of this time point is 4 min. Evaporation of the polymer-lean phase may occur earlier in the middle of the coating (in the width direction) because the skin might be thinnest there and the resistance to evaporation is low. Near the edges, however, the skin might be thicker, causing more resistance to evaporation. These differences were not easily detected from SEM images.

Fig. 7 shows SEM micrographs of the final microstructure of the CA/A/W coating. The structure consists of a dense skin ~0.1 μm thick atop a porous substructure with pore sizes ranging from 0.5–2 μm. The pores appear ellipsoidal, with the major axis parallel to the plane of the substrate. This pore shape is likely due to shrinkage of the coating in the thickness direction during drying. The top surface appears continuous and shows little microstructure, and the bottom surface is continuous except for a few small (<1 μm) pores.

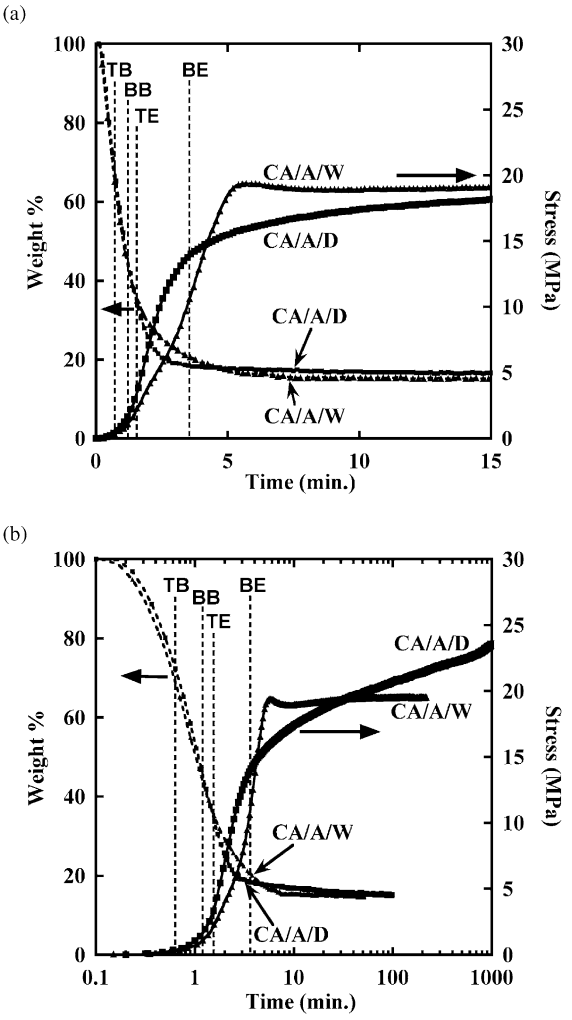

Fig. 8. Stress evolution (—) and weight loss (- - -) as a function of drying time for a non-phase-separating coating initially composed of CA/A/D (10/80/10) (■) and a phase-separating coating composed of CA/A/W (10/80/10) (▲). Final thickness for CA/A/W (porous) coating was ~23 μm. Vertical dashed lines (for CA/A/W): (TB) translucency begins at clamped end; (BB) bright white begins at clamped end; (TE) translucent over entire coating; (BE) bright white over entire coating. (a) linear scale at early time; (b) log scale to show differences in behavior over a long time scale.

The stress evolution curves and the drying curves for the CA/A/D and CA/A/W coatings are shown in Fig. 8. The time points for the optical changes for the CA/A/W coating are also shown. The weight loss and stress data in the very beginning stages of drying (less than 1 min) are nearly identical. After this time, drying of the CA/A/W slows and significant differences in the stress data appear. The stress profile for the CA/A/W coating shows an initial slower rise in stress (compared to the CA/A/D coating), followed by a maximum in stress (at ~5 min) and a short period of decreasing stress before reaching a fairly constant stress level of ~20 MPa. Toward the latter stages of drying, the CA/A/W coating reaches a more constant weight compared with the CA/A/D coating, which continues to dry slowly and accumulate stress. Key differences between coatings

are: (i) a stress maximum and subsequent period of stress relaxation were apparent for the CA/A/W coating and (ii) the final coating stress is lower in the CA/A/W coating. In the following paragraphs, these differences in stress and weight loss for the two coatings are discussed.

Early in drying ($t < \sim 1$ min), the two coatings have roughly the same stress and weight loss profiles. Acetone evaporation dominates in both coatings because it is much more volatile than dioxane or water. Stress becomes apparent in both coatings at around the 25 s time point. Between ~40 s and 1 min of drying, the weight loss and stress curves continue to overlap even though the CA/A/W coating has started to phase separate near the edges and the clamped end of the substrate.

In the CA/A/W coating, phase separation and drying occur simultaneously. As drying proceeds, the compositions and relative amounts of the polymer-rich and polymer-lean phases change and the coating microstructure evolves. Using cryo-microscopy, Prakash [33] observed the microstructures of CA/A/W coatings at different stages of drying. He found that polymer-lean droplets form initially in a polymer-rich matrix, and then with more drying, these droplets merge into a continuous polymer-lean phase, which is eventually replaced by air. A dense skin was also found throughout drying.

As stated in Section 3.1, stress depends on the shrinkage of the coating after solidification and the evolving coating modulus; phase separation affects both quantities and hence the stress. After phase separation, the coating is a composite consisting of polymer-rich and polymer-lean phases; therefore, the overall coating modulus depends on the modulus of each phase and their relative amounts. The measured coating stress is due to the constrained shrinkage of the entire coating, but local stresses can also develop. The formation and evolution of the polymer-lean phase involves the removal of solvent and nonsolvent from the polymer-rich matrix. This process leads to shrinkage of the polymer-rich phase and a local tension in this phase.

As evaporation proceeds further (1–3 min of drying), differences in drying and stress development appear. After 1 min of drying, the coating that phase separates (CA/A/W) begins to dry more slowly. The slower drying may be related to the higher polymer concentration (and hence lower solvent and nonsolvent diffusivity) in the polymer-rich phase of this coating, compared with coating which remains a single phase (CA/A/D). During this time period, the CA/A/W coating also turns bright white as the polymer-lean phase evaporates and air-filled voids are left behind. Due to the dense skin, evaporation of the polymer-lean phase requires diffusion of acetone and water through the polymer-rich phase, which for reasons cited above may be slower than the diffusion through the homogeneous CA/A/D coating. Stress is also lower in the CA/A/W coating during this time period (~1–3 min). The phase separation in the CA/A/W coating delays the climb in the stress in the first few minutes of drying for two reasons. First, the coating shrinks less, initially because the coating is drying more slowly and later because the removal of volatiles results in pores rather than shrinkage of the coating. Second, the coating modulus is likely lower throughout drying due to the presence of a low-modulus polymer-lean phase and then, eventually, air. The greater final coating thickness of the CA/A/W coating (24 μm) compared to that of the CA/A/D coating (20 μm) is caused by porosity.

At a later stage (after 3 min), drying and stress development in the CA/A/W coating continues and then the weight and stress level off to a constant value, while drying and stress development in the CA/A/D coating continues for a longer time at a slower rate. For the CA/A/W coating, weight loss continues even after the coating appears entirely bright white because the polymer-rich phase continues to lose solvent and the coating may dry (and the pores empty) nonuniformly through the thickness. Stress rises quickly in the CA/A/W coating at this stage of drying, because the steady solvent loss leads to more shrinkage in the coating; pores collapse and the coating modulus increases, further enhancing stress development. The coating weight becomes stable sooner for the CA/A/W coating because solvent and nonsolvent may be transported out of the thin polymer-rich regions through the air-filled, interconnected voids and then eventually through the thin polymer-rich skin. In CA/A/D, the solvents must diffuse through the dense polymer coating, a slower process in the late stages of drying when the coating is glassy and the diffusivity is large. Stress continues to rise at a steady rate in CA/A/D coating reaching 23 MPa after 16 h of drying (Fig. 8b). The higher final stress in the CA/A/D coating is due to its higher modulus and its greater shrinkage.

The discussion above focuses on stresses due to constrained shrinkage; however, the effect of capillary pressure on stress must also be considered in drying coatings that contain liquid-filled pores. This effect can be analyzed using the Young–Laplace equation (assuming a contact angle equal to zero):

$$P_C = 2\gamma/r \tag{3}$$

where P_C is the capillary pressure, γ is the surface tension of the interstitial fluid, and r is the radius of the pore throat. Capillary pressure, in addition to shrinkage from solvent removal, causes the coating to contract. Assuming the interstitial liquid contains mainly water and that the pore throat radius is about 1 μm (as shown in Fig. 7), then $P_C \approx 0.14$ MPa, a value much smaller than the measured stresses in this study. Therefore, the primary source of stress in these porous coatings is from shrinkage. In other coatings, however, in which the pores are smaller, capillary pressure can significantly contribute to the overall stress level, as seen by other researchers [34–37].

Capillary pressure, therefore, does not contribute greatly to the overall stress magnitude in the porous coating; however, it likely contributes to the different type of stress profile for this coating. Specifically, a stress maximum and

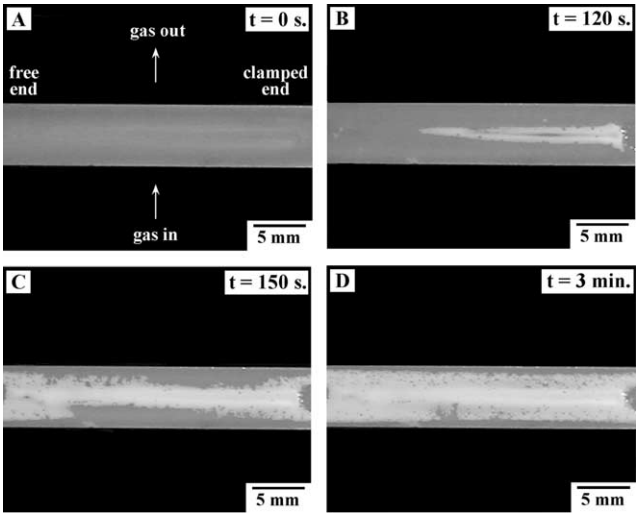

Fig. 9. Images of the surface of a coating prepared from CA/A/W (10/65/25), captured from a real time video. Time points indicated in the upper right of each image.

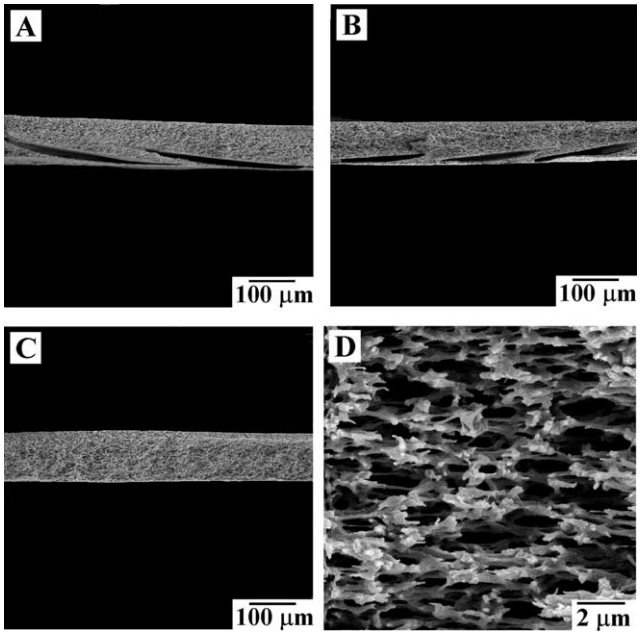

Fig. 10. SEM images showing the final microstructure in cross-sectional view of the coating prepared from CA/A/W (10/65/25): (A) large voids about 3/4 the distance to the left of the coating center (in the width direction); (B) large voids about 3/4 the distance to the right of the coating center; (C) large voids not present in the center of the coating; (D) higher magnification of (C).

subsequent stress relaxation are apparent. For the porous coating, a liquid–vapor meniscus develops at some point during drying. As the polymer-lean phase continues to evaporate, capillary forces, which compress the porous coating, release. The stress relaxation for the porous coating is probably due to the retreating meniscus. In fact, the amount of stress relaxation measured for the porous coating (Fig. 8) is ~0.5 MPa, which is on the same order of magnitude as the capillary pressure calculated using Eq. (3). This theory to explain the stress maximum and subsequent stress relaxation in porous coatings is supported by other researchers. Chiu and Cima [34] observed that the stress maximum seemed to coincide with the disappearance of the supersaturated regime (i.e. 100% saturation) in binder-free ceramic particulate coatings. Similar stress behavior was also reported for other porous coatings including tape-cast porous ceramic coatings [35] and latex coatings [21,37,38].

In summary, there are differences in the weight loss and stress profiles for the dense and porous coatings. The weight loss profile for the porous coating shows a delayed weight loss, followed by a period of faster weight loss. The stress profile for the porous coating features a delayed rise in stress, and then a steeper rise. For the porous coating, a stress maximum and subsequent period of stress relaxation were apparent; the relaxation is attributed to capillary pressure relief from pore emptying.

3.3. Large void formation

In this section, the stress and drying behavior of a coating that forms both large voids and small pores is considered. Fig. 9 shows top views (obtained with a video camera) during drying of a coating prepared from a polymer solution initially containing 10 wt% CA, 65 wt% acetone, and 25 wt% water (referred to here as 10/65/25). The coating appeared translucent almost immediately upon deposition; from the position of the initial composition on the phase diagram, one might expect this structure to form by spinodal decomposition. At around the 110 s time point, the coating began to change from translucent to bright white, starting at the clamped end, then moving down the center (in the width direction) of the coating toward the free end, and then gradually moving outward from the center toward the edges. The coating appeared to be bright white over its entire area by around the 3 min time point. As described in Section 3.2, the translucent appearance signals phase separation and the bright white appearance corresponds to the formation of air-filled voids.

Fig. 10 shows the final microstructure of this coating. The structure consists of a dense skin (not shown, ~0.1 μm thick) atop a microporous (pore size ~0.5–2 μm) substructure. Large voids (~200–300 μm long) are also evident in the microstructure. These large voids appear more slanted than macrovoids previously published in the literature prepared via the dry-cast process [6,17,39]; one reason for this shape may be that the coatings in this study are thinner. When thicker coatings were prepared, the shape appeared more vertical. The large voids are found in approximately half of the coating and located closest to the edges (i.e. along the 6.5 mm width of the coating, macrovoids are found at ~0–1.6 mm and ~4.9–6.5 mm).

The stress evolution and drying data for the CA/A/W (10/65/25) are shown in Fig. 11. For comparison, the stress and weight loss data for the CA/A/W (10/80/10) coating from

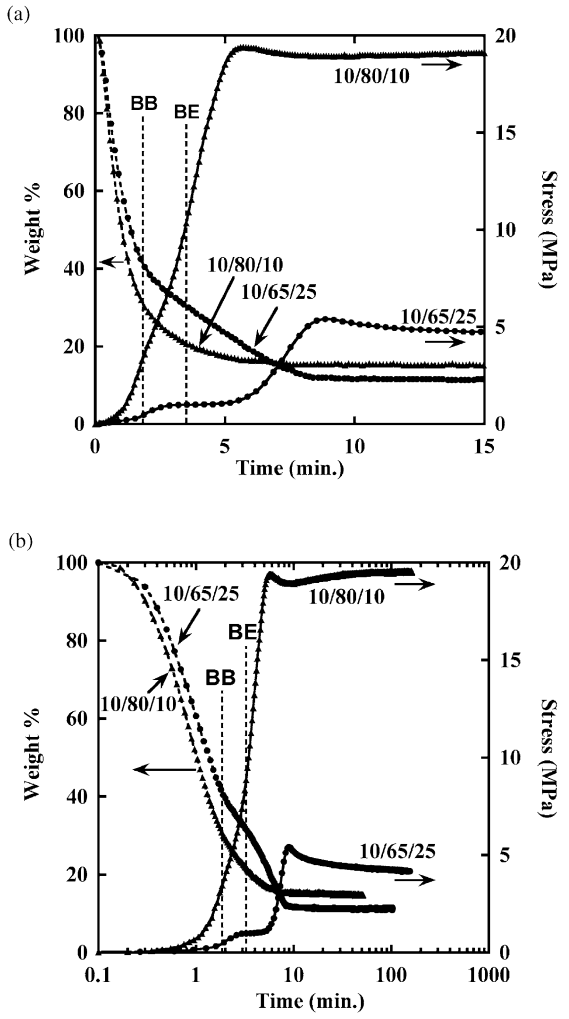

Fig. 11. Stress evolution (—) and weight loss (- - -) as a function of drying time for two phase-separating coatings initially composed of CA/A/W (10/80/10) (▲) and CA/A/W (10/65/25) (●). Final thickness for 10/65/25 coating was ~57 μm. Vertical dashed lines (for 10/65/25): (BB) bright white begins at clamped end; (BE) bright white over entire coating. (a) linear scale at early time; (b) log scale to show differences in behavior over a long time scale.

Section 3.2 are also plotted. During the first 2 min, the weight loss and stress behaviors for these two coatings are similar, but the 10/65/25 coating loses weight and develops stress more slowly compared with the 10/80/10 coating. After ~2 min of drying, the rate of weight loss for the 10/65/25 coating slows, and after ~10 min, the weight levels off to 11% of the original coating weight (a lower value than that for the 10/80/10 coating). The stress curve for the 10/65/25 coating shows that stress rises slowly from the 40 s time point to the 2.5 min time point, when it levels off to ~1 MPa. Stress is constant at 1 MPa for a few minutes, then it increases again, and then finally it relaxes to ~4 MPa. The most notable differences in the stress behavior for the two coatings are: (i) the stress in the 10/65/25 coating rises more slowly and reaches a plateau at ~1 MPa, and (ii) the final stress in the 10/65/25 coating is about four times lower than in the 10/80/10 coating.

Early in the drying process (<2 min), the 10/65/25 coating loses weight and develops stress more slowly than the 10/80/10 coating. The slower drying is probably related to the higher water content in the 10/65/25 coating. The slower stress development in this coating may be explained as follows. Less time for solvent and nonsolvent evaporation is required for the coating composition to enter the two-phase region of the ternary phase diagram (Fig. 1) and the coating phase separates quickly (Fig. 9). Therefore, the cellulose acetate concentration in the polymer-rich phase of the 10/65/25 coating is much lower than the cellulose acetate concentration in the 10/80/10 coating upon phase separation (which occurs after ~40 s of drying). Shojaie et al. [6,39] predicted drying path trajectories through the CA/A/W ternary phase diagram during the dry-cast process for initial compositions similar to the ones in this study; their model predictions confirm the idea presented here that the polymer-rich phase of the 10/65/25 coating has a lower concentration of cellulose acetate upon phase separation. This causes the polymer-rich phase in the 10/65/25 coating to have a lower modulus than the polymer-rich phase of the 10/80/10 coating; therefore, it is weaker and is not able to support as much coating stress.

The drying rate for the 10/65/25 coating slows at about the 2 min time point, coincident with the beginning of the transition to a bright white appearance. The change in drying rate probably indicates that water has become the primary component that evaporates from the coating. The bright white transition indicates that the polymer-lean phase, consisting of mainly water, has started to evaporate.

The most striking difference in stress behavior between the two coatings is the plateau in stress from ~2.5 to 6 min for the 10/65/25 coating at ~1 MPa. During this period, the stress remains constant even though weight loss continues. Therefore, either this weight loss occurs with no shrinkage in the coating or the stress that should develop from shrinkage is able to relax by some mechanism. Some of the weight loss that occurs during this period is from evaporation of the polymer-lean phase (pore emptying), which probably does not lead to much shrinkage and hence has little effect on the stress. However, solvent and nonsolvent are also being removed from the polymer-rich phase, which should cause the coating to shrink and the stress to increase. It is proposed here that the stress caused by the removal of solvent and nonsolvent from the polymer-rich phase is relaxed by the formation and growth of macrovoids by rupture of the polymer-rich phase. As mentioned in the previous paragraph, it is likely that the 10/65/25 coating has a lower modulus than the 10/80/10 coating, which would make it easier for the polymer-rich phase to rupture. In support of this idea, cryomicroscopy work by other researchers has confirmed that phase separation occurs before macrovoid formation [33,40].

At ~6 min of drying, stress in the 10/65/25 coating begins to increase once again. Because the modulus of the polymer-rich phase grows continuously as drying proceeds,

a point is reached at which the modulus is large enough so that the polymer-rich phase can support more stress without rupturing. The increase in stress starting at 6 min indicates that stress is again growing due to constrained shrinkage and modulus growth. Stress stops rising by ~9 min of drying; at about this time, the corresponding weight loss curve begins to level off. Again, the stress relaxation apparent after the 9 min time point is probably due to capillary pressure relief from pore emptying.

Here it is proposed that macrovoids are caused by rupture of the weak polymer-rich phase due to the stress generated from solvent and nonsolvent loss. The fact that macrovoids form in the 10/65/25 coating and not the 10/80/10 coating may be explained using the same argument discussed above: for the 10/65/25 coating, the cellulose acetate concentration in the polymer-rich phase is lower than the cellulose acetate concentration in the 10/80/10 coating upon phase separation, which in turn causes the polymer-rich phase in the 10/65/25 coating to have a lower modulus. Therefore, it is weaker and is not able to support much coating stress. For the 10/65/25 coating, the polymer-rich phase ruptured once the critical stress of 1 MPa was reached. In fact, a plateau in stress at 1 MPa was present for other macrovoid-containing 10/65/25 coatings prepared under slightly different conditions (higher relative humidity (27%), smaller coating thickness (~40 μm), and larger coating thickness (~80 μm)), indicating that 1 MPa of coating stress is the critical stress level for the polymer-rich phase.

The fact that macrovoids are more common during the wet-cast process [6] agrees with this theory that macrovoids form in coatings that have a weak polymer-rich phase. During the wet-cast process, the polymer solution is cast on a substrate and immersed in a coagulation bath containing a nonsolvent. Phase separation via the wet-cast process occurs because of the exchange of solvent for nonsolvent. After phase separation occurs in the wet-cast process, the polymer-rich phase continues to lose some solvent, but it can also gain nonsolvent; in the dry-cast process, the polymer-rich phase loses *both* solvent and nonsolvent. Therefore, the modulus of the polymer-rich phase obtained via the wet-cast process is probably lower, causing it to be more susceptible to rupture from shrinkage stress (caused in this case by unequal exchange of solvent and nonsolvent with the coagulation bath).

There are several theories proposed in the literature to explain macrovoid formation; however, only a few researchers have proposed that shrinkage stress may be a cause. Gröbe and Meyer [41] proposed that macrovoids result from rupture of the internal structure caused by a rigid skin and subsequent pressure produced from inward diffusion. Frommer and Lancet [42] proposed that the polymer-rich phase has a tendency to shrink, and that opposing adhesive constraints may play a role. Strathman and Kock [13] and Altena [43] proposed that macrovoids form from defects in the skin layer during the wet-cast process. According to this view, shrinkage stress in the solidified polymer skin, which cannot be relieved by relaxation of the polymer, causes the homogeneous polymer layer to rupture. Shrinkage of the polymer matrix then causes the void to grow by draining freshly precipitated polymer at the bottom of the macrovoid to the side of the macrovoid. Time-sectioning cryogenic microscopy studies by Prakash [33] led to a theory involving the progressive rupture of the polymer-rich phase, which is similar to Frommer and Lancet's view. The results presented in the present work agree with the macrovoid growth mechanism all of these researchers proposed.

Several factors may be responsible for the lower final stress in the 10/65/25 coating. First, rupture of the polymer-rich phase to form macrovoids relieves some of the stress in this coating, as described above. Second, the overall shrinkage in this coating is lower: the final coating thickness of the 10/65/25 coating (57 μm) is greater than that of the 10/80/10 coating (24 μm). Finally, the modulus of the 10/65/25 coating is likely lower due to the presence of the large voids.

4. Conclusions

The tensile stress development during drying of cellulose acetate (CA) coatings prepared from binary and ternary cellulose acetate solutions was measured by a cantilever deflection technique. Results from dense coatings, a microporous coating, and microporous coating that also contained larger voids were compared. The porous microstructures were induced by phase separation. Stress in these porous coatings results from constrained shrinkage of the coating during drying. The final stress was highest in the dense coating and lowest in the coating that contained large voids and small pores. For the porous coatings, a period of stress relaxation was apparent and is attributed to capillary pressure relief from pore emptying. The stress profile for the coating that contained large voids and small pores was quite different than the other coatings in this study because it showed a plateau in stress early in the drying process. It is proposed that during the plateau period, stress generated due to solvent and nonsolvent loss from the polymer-rich phase is relieved by the growth of the larger voids.

The present results give a better understanding for the mechanisms responsible for coating stress in porous polymeric coatings prepared using the dry-cast phase separation method. These results will be useful in the design of processing schedules for preparing asymmetric membranes.

Acknowledgements

The authors acknowledge the University of Minnesota Graduate School, through its Doctoral Dissertation Fellowship, and the Industrial Partnership for Research in Interfacial and Materials Engineering along with its industrial supporters, through the Coating Process Fundamentals

Program, for financial support of this research. The authors also acknowledge K. Zhang for his expertise and help with SEM imaging and T. Baraniak and W. Suszynski for their technical assistance. Finally, helpful discussions with C. Miller are gratefully acknowledged.

References

[1] Wicks ZW, Jones FN, Pappas SP. Organic coatings: science and technology. New York: Wiley, 1992. Chapter 14.
[2] Dabral M. Solidification of coatings: theory and modeling of drying, curing, and microstructure growth. PhD Thesis. University of Minnesota, Minneapolis, MN, 1999.
[3] Dabral M, Francis LF, Scriven LE. AIChE Journal 2002;48(1)25–37.
[4] Tsujimoto T. Solution film casting technology. Proceedings of the 9th International Coating and Technology Symposium. International Society of Coating Science and Technology, Newark, DE, 1998.
[5] Kesting RE. J Appl Polym Sci 1973;17:1771–84.
[6] Shojaie SS, Krantz WB, Greenberg AR. J Membr Sci 1994;94: 281–98.
[7] Mulder M. Basic principles of membrane technology. Dordrecht, The Netherlands: Kluwer Academic Publishers, 1991. Chapters 1–3.
[8] van de Witte P, Dijkstra PJ, van den Berg JWA, Feijen J. J Membr Sci 1996;117:1–31.
[9] Strathmann H. ACS Symp Ser 1985;269:165–95.
[10] Strathmann H, Scheible P, Baker RW. J Appl Polym Sci 1971;15: 811–28.
[11] Lonsdale HK. J Membr Sci 1982;10:81–181.
[12] Smolders CA, Reuvers AJ, Boom RM, Wienk IM. J Membr Sci 1992;73:259–75.
[13] Strathmann H, Kock K, Amar P. Desalination 1975;16:179–203.
[14] Strathmann H, Kock K. Desalination 1977;21:241–55.
[15] Ray RJ, Krantz WB, Sani RL. J Membr Sci 1985;23:155–82.
[16] Boom RM, Wienk IM, van der Boomgaard T, Smolders CA. J Membr Sci 1992;73:277–92.
[17] Zeman L, Fraser T. J Membr Sci 1993;74:93–106.
[18] Paulsen FG, Shojaie SS, Krantz WB. J Membr Sci 1994;91:265–82.
[19] Croll SG. J Coat Technol 1978;50(638):33–8.
[20] Sato K. Prog Org Coat 1980;8:143–60.
[21] Perera DY, Eynde DV. J Coat Technol 1984;56(717):47–53.
[22] Payne JA, Francis LF, McCormick AV. J Appl Polym Sci 1997;66: 1267–77.
[23] Croll SG. J Appl Polym Sci 1979;23:847–58.
[24] Croll SG. J Coat Technol 1980;52(665):847–58.
[25] Perera DY, Eynde DV. J Coat Technol 1981;53(677):39–44.
[26] Tong HM, Hu CK, Feger C, Ho PS. Polym Engng Sci 1986;26(17): 1213–7.
[27] Payne JA. Stress evolution in solidifying coatings. PhD Thesis. University of Minnesota, Minneapolis, MN, 1998.
[28] Payne JA, Francis LF, McCormick AV. Rev Sci Instrum 1997;68(12): 4564–8.
[29] Stoney GG. Proc R Soc 1909;A82:172.
[30] Timoshenko SP, Gere JM. Theory of elastic stability. New York: McGraw Hill, 1961. Chapter 6.
[31] Corcoran EM. J Paint Technol 1969;41(538):635–40.
[32] Hoffman RW. Surf Anal 1981;3:62–6.
[33] Prakash SS. The origins of microstructure in phase inversion coatings or membranes: snapshots of the transient from time-sectioning cryo-sem. PhD Thesis. University of Minnesota, Minneapolis, MN, 2001.
[34] Chiu RC, Cima MJ. J Am Ceram Soc 1993;76(11):2769–77.
[35] Lewis JA, Blackman KA, Ogden AL, Payne JA, Francis LF. J Am Ceram Soc 1996;79(12):3225–34.
[36] Daniels MW. Colloidal ceramic coatings with silane coupling agents. PhD Thesis. University of Minnesota, Minneapolis, MN, 1999.
[37] Petersen C, Heldmann C, Johannsmann D. Langmuir 1999;15: 7745–51.
[38] Perera DY. J Coat Technol 1984;56(716):111–8.
[39] Shojaie SS, Krantz WB, Greenberg AR. J Membr Sci 1994;94: 255–80.
[40] Limbert A. Microstructure development in coatings by cryogenic scanning electron microscopy. MS Thesis. University of Minnesota, Minneapolis, MN, 1996.
[41] Grobe V, Meyer K. Faserforsch u Textiltech 1959;10:214–24.
[42] Frommer MA, Lancet D. In: Lonsdale HK, Frommer MA, editors. Lancet Ds reverse osmosis in membrane research. New York: Plenum Press, 1972. p. 85–110.
[43] Altena F. Phase separation phenomena in cellulose acetate solutions in relation to asymmetric membrane formation. PhD Thesis. Twente University of Technology, Enschede, Netherlands, 1982.